1 Introduction

Hydrogen has great potential as a carbon-alternative fuel for both the energy and aviation industries. However, due to its chemical reactivity, it is a highly unstable fuel alone. Hydrogen-ammonia blends have been shown to minimize the high reactivity and mitigate the logistical risks of transporting and storing hydrogen alone.

The purpose of this study is to validate the combustion properties of partially decomposed ammonia blends and compare the combustion properties to traditional methane fuels. We use the mixture averaged transport model in Cantera, assuming a nonunity lewis number, in order to observe flame stretch effects.

Cantera was used to validate a chemical kinetics mechanism with 32 species and 165 reactions. A spatial convergence study of a Direct Numerical Simulation using NGA, a finite difference code, was conducted for a laminar premixed flame propagating steadily across a spatial domain.

2 Mole Fractions

Given the stoichiometric mole fractions of $NH_3, H_2, and N_2$ along with the equivalence ratio, the actual mole fractions are determined and a script was created.

The $NH_3/H_2/N_2$ combustion reaction is

$$\frac{(1-\gamma)\mathrm{NH_3}}{1+\gamma} + \frac{3\,\gamma \mathrm{H_2}}{2\,(1+\gamma)} + \frac{\gamma \mathrm{N_2}}{2\,(1+\gamma)} + \mathrm{x}(0.21\,\mathrm{O_2} + 0.79\,\mathrm{N_2}) \longrightarrow \mathrm{y}H_2O + \mathrm{z}N_2. \tag{1}$$

and the fuel-to-air ratio is found by

$$\frac{x}{\phi} = \frac{\eta_A}{\eta_F}. \tag{2}$$

We define

$$\eta_{\mathrm{NH_3^i}} = \text{the initial moles of ammonia.}$$
$$\eta_{\mathrm{NH_3^c}} = \text{the decomposed moles of ammonia.}$$
$$\eta_{\mathrm{NH_3^f}} = \text{the remaining moles of ammonia.}$$
$$\gamma = \frac{\eta_{\mathrm{NH_3^c}}}{\eta_{\mathrm{NH_3^i}}}.$$

To find x, y, and z, we balance the H, O, and N atoms for the products and reactants:

$$H : \frac{3(1-\gamma)}{(1+\gamma)} + \frac{3\gamma}{1+\gamma} = 2y \tag{3}$$

$$y = \frac{3}{2(1+\gamma)} \tag{4}$$

$$O : \frac{3\gamma}{2(1+\gamma)} = 2(0.21)x \tag{5}$$

$$x = \frac{3.571}{1+\gamma} \tag{6}$$

$$N : \frac{(1-\gamma)}{(1+\gamma)} + \frac{\gamma}{2(1+\gamma)} + \frac{0.79(2)(3.571)}{1+\gamma} = 2z \tag{7}$$

$$z = \frac{(6.64 - \frac{\gamma}{2})}{2(1+\gamma)} \tag{8}$$

Therefore, Equation 1 becomes

$$\frac{(1-\gamma)\mathrm{NH_3}}{1+\gamma} + \frac{3\,\gamma \mathrm{H_2}}{2\,(1+\gamma)} + \frac{\gamma \mathrm{N_2}}{2\,(1+\gamma)} + \frac{3.571}{\phi(1+\gamma)}(0.21\,\mathrm{O_2} + 0.79\,\mathrm{N_2}) \longrightarrow \frac{3\,\mathrm{H_2O}}{2\,(1+\gamma)} + \frac{(6.64 - \frac{\gamma}{2})\mathrm{N_2}}{2\,(1+\gamma)}. \tag{9}$$

The analysis is continued to find the total moles of each of the constituents on the reactants side:

$$\eta_{\mathrm{NH_3}^f} : \frac{(1-\gamma)}{(1+\gamma)} \tag{10}$$

$$\eta_{\mathrm{H_2}} : \frac{3\gamma}{2(1+\gamma)} \tag{11}$$

$$\eta_{\mathrm{O_2}} : \frac{0.75}{\phi(\gamma+1)} \tag{12}$$

$$\eta_{\mathrm{N_2}} : \frac{\gamma}{2(1+\gamma)} + \frac{3.571(0.79)}{\phi(1+\gamma)} = \frac{5.64 + \phi\gamma}{2\phi(1+\gamma)} \tag{13}$$

$$\tag{14}$$

The total number of moles in the product mixture, η_{tot}, is defined as

$$\eta_{tot} = \eta_{\mathrm{N_2}} + \eta_{\mathrm{H_2}} + \eta_{\mathrm{O_2}} + \eta_{\mathrm{NH_3^f}} = 1 + \frac{3.571}{\phi(1+\gamma)} \mathrm{moles}. \tag{15}$$

From here, the mole fractions of each reactant from 9 is

$$X_{species} = \frac{\eta_{species}}{\eta_{tot}}. \tag{16}$$

3 Kinetic Modeling Study

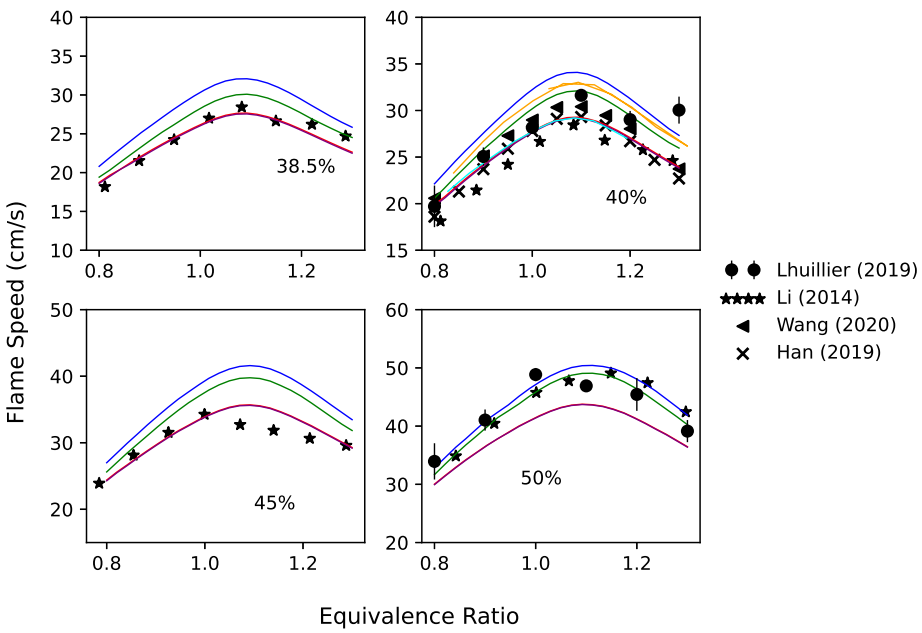

Figure 1: Laminar flame speed vs equivalence ratio of an NH_3/H_2-air mixture at p = 1 atm, T = 298.15 K for different mole fractions of H_2. Our simulation results from the Gotama mechanism in red and our results from the Stagni mechanisms from 2020 and 2023 in green and blue, respectively, are compared against simulation data from the Stagni paper (2023). In addition, results from the Gotama mechanism with radiation enabled are plotted in purple.

The experimental data from Han et al. (2019) agrees most strongly with the results found using the Gotama mechanism.

While the results from Li agreed decently with the Gotama mechanism for X_{H_2}=0.385, there is a strange dropoff in the their values of laminar flame speed for X_{H_2}=0.45 after for values of $\phi > 1.0$. Li et al. made no notice of this in their paper, but mentioned that the laminar flame speeds at X_{H_2}=0.45 are similar to that of methane-air flames. It is worth noting that Li's datapoints for $X_{H_2} = 0.45$ are the only ones they supplied that exhibit this drop-off behavior.

Li et al. also mention that their experiments overpredict the burning velocity at X_{H_2}=0.5 because they did not consider stretch effects in their experiments, which may explain why the most significant disagreement between their data and the data from the Gotama mechanism is at X_{H_2}=0.5.

The data from Li et al. was sourced from their paper, while experimental data from all other sources in Figure **??** was sourced from the authors' supplementary material.

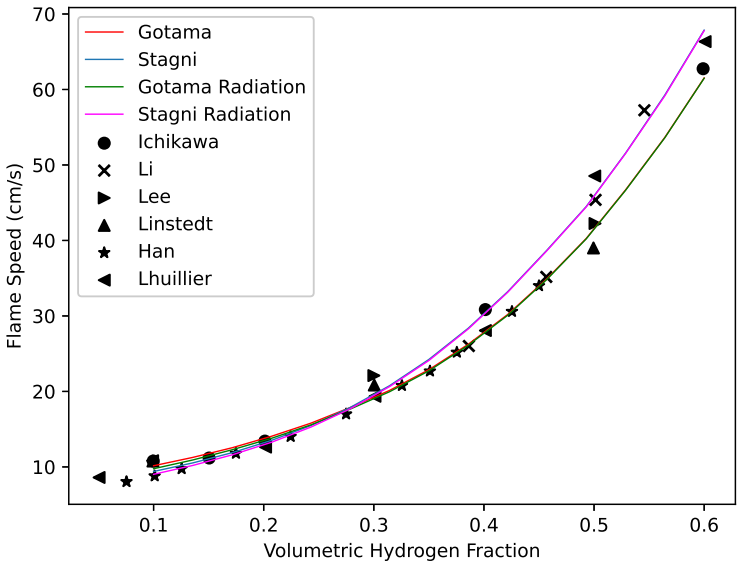

Figure 2: Laminar flame speed vs volumetric hydrogen fraction of a NH_3/H_2-air mixture at p = 1 atm, T = 298.15 K, $\phi = 1.0$. Simulation results from the Gotama mechanism are plotted in red, while results from the Stagni mechanism are in blue. Results from the Gotama mechanism and Stagni mechanism with radiation enabled are plotted in green and magenta respectively.

The discrepancy between Dr. Stagni's laminar flame speed results, which were computed with OpenSMOKE, and the Cantera results for a laminar ammonia-air flame are investigated. Previously, the Cantera simulations did not account for radiation at all.

It is evident from Nakamura et al. (2019) that radiation does have an impact on flames of NH_3/air, especially at values greater than or less than $\phi = 1.0$. However, this difference is around 4-5 cm/s, which is within most experimental uncertainty bounds. Dr. Stagni included H_2O as a radiating species in his 2023 paper, so by enabling radiation in Cantera, we similarly account for H_2O radiation.

The laminar flame speed data from the Gotama paper was digitized for $X_{H_2} = 0.4$ and is shown in cyan. There is good agreement between our results obtained with the Gotama mechanism and the data from the Gotama paper. This suggests that our simulation setup is equivalent to Gotama's.

Figure 2 shows that there is a very slight change in the flame speed at lower values of X_{H_2} for both the Stagni and Gotama mechanisms. This change is in accordance with the results from the Nakamura paper, where the effect of radiation on laminar flame speed is existent but very small. In general, radiative effects on laminar flame speed are negligible at higher values of X_{H_2}.

4 Results

4.1 NH3/air mixtures

I used pressure values from 1.0-4.0 atm, hydrogen fraction values from 0.4-0.5, and equivalence ratio values from 1.0-1.3.

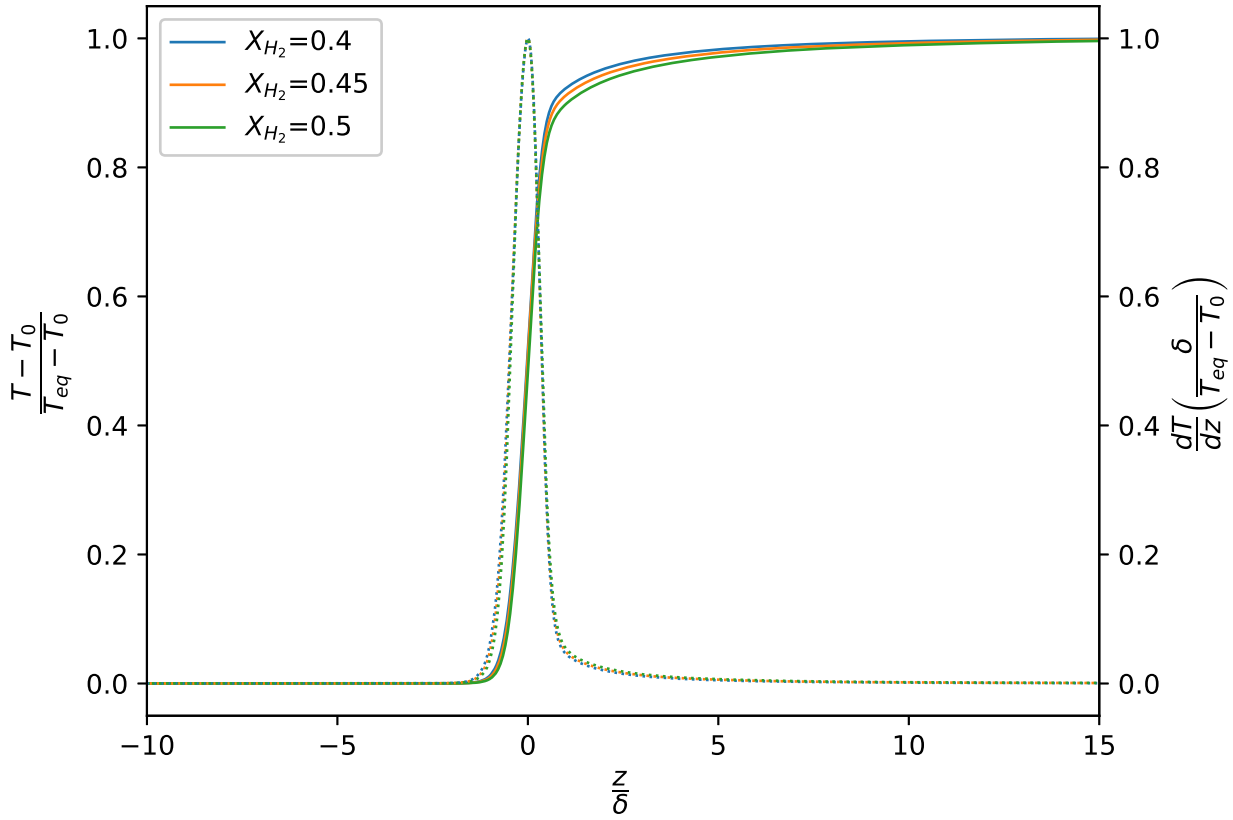

Figure 3: Temperature profile for an ammonia-air laminar flame with $T_0 = 298.15$ K, $\phi = 1.0$, and $p = 1.0$ atm with varying X_{H2} values.

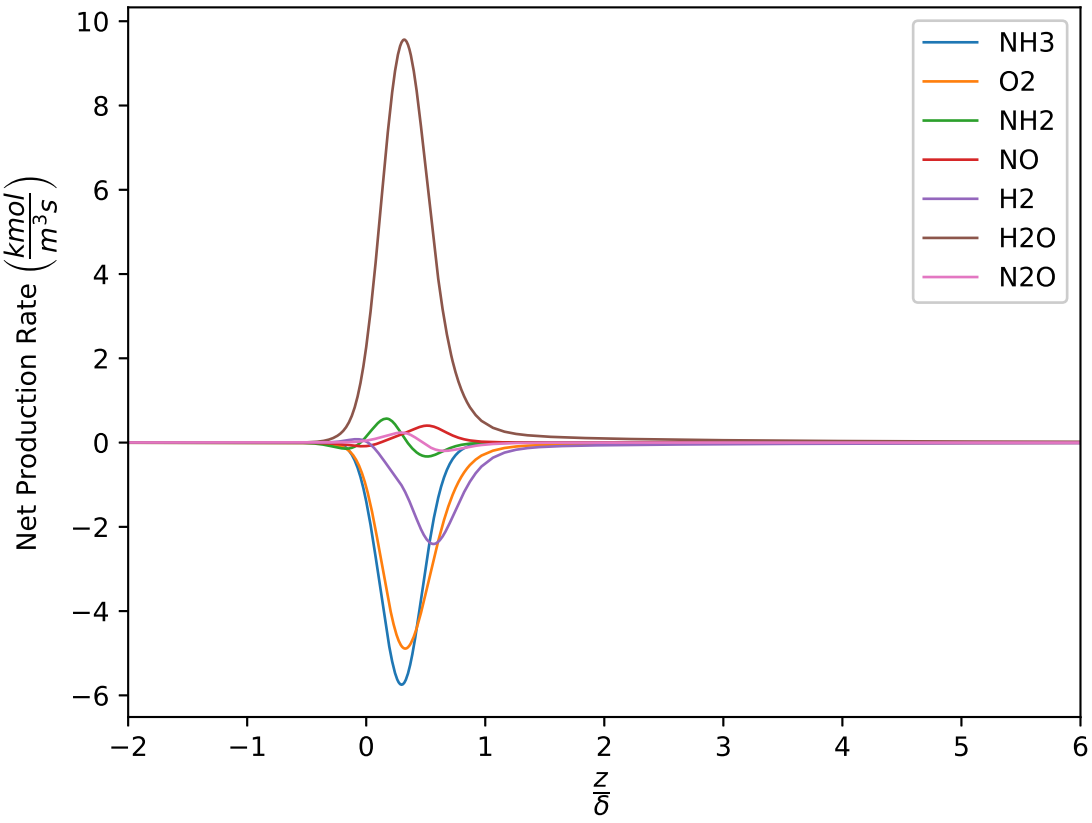

Figure 4: Molar production rates for an ammonia-air laminar flame with $T_0 = 298.15$ K, $\phi = 1.0$, $p = 1.0$ atm, and $X_{H2} = 0.4$.

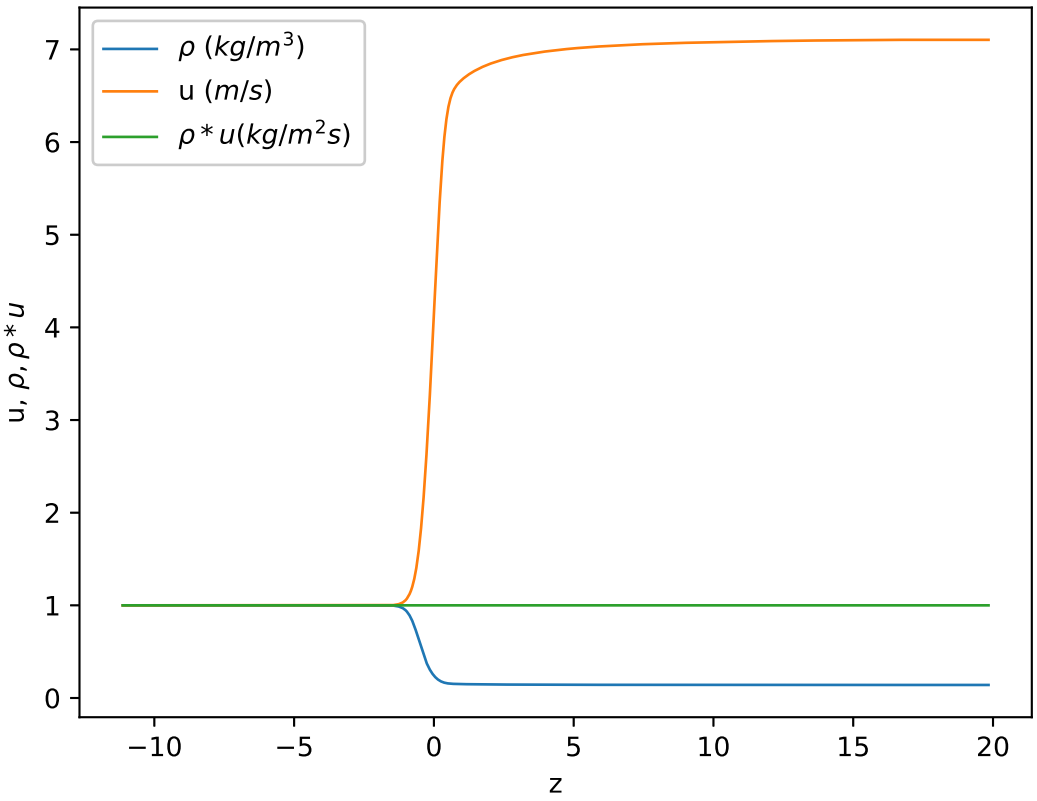

Figure 5: Mass flow rate for an ammonia-air laminar flame with $T_0 = 298.15$ K, $\phi = 1.0$, $p = 1.0$ atm, and $X_{H2} = 0.4$.

4.2 CH4-air flames

I simulated a fuel-lean methane-air laminar flame using the uberFlame.py script. I assumed that the slope of the temperature curve was linear to approximate its slope $\frac{dT}{dz}$.

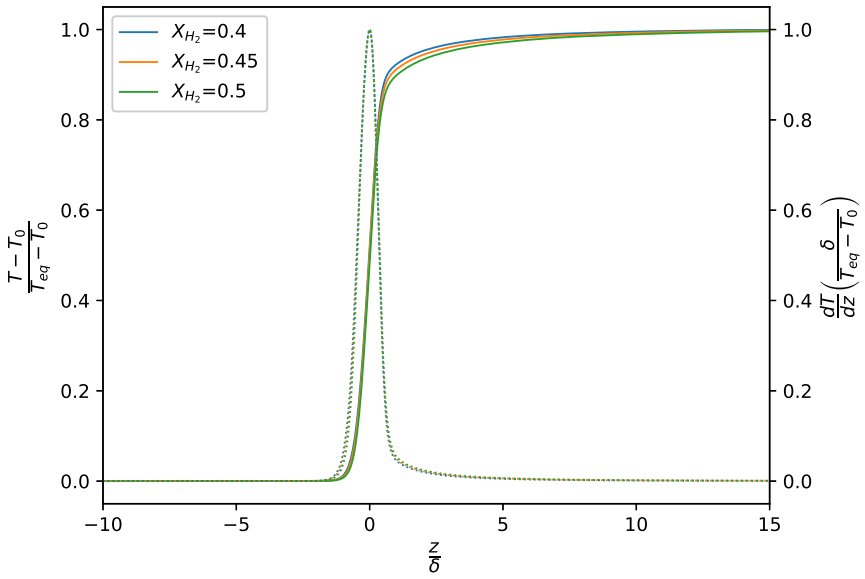

Figure 6: Temperature profile for a methane-air laminar flame with T_0=800K, p=4 atm, ϕ=0.7.

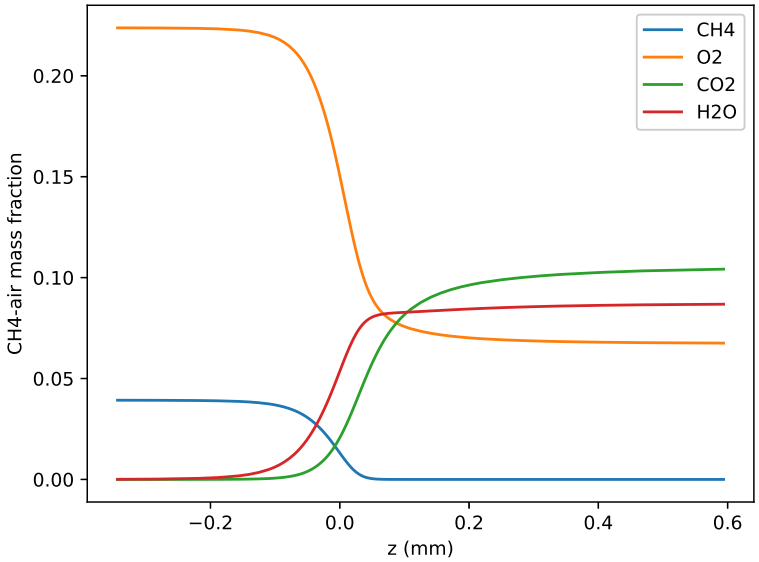

Figure 7: Composition profile for a methane-air laminar flame with T_0=800K, p=4 atm, ϕ=0.7.

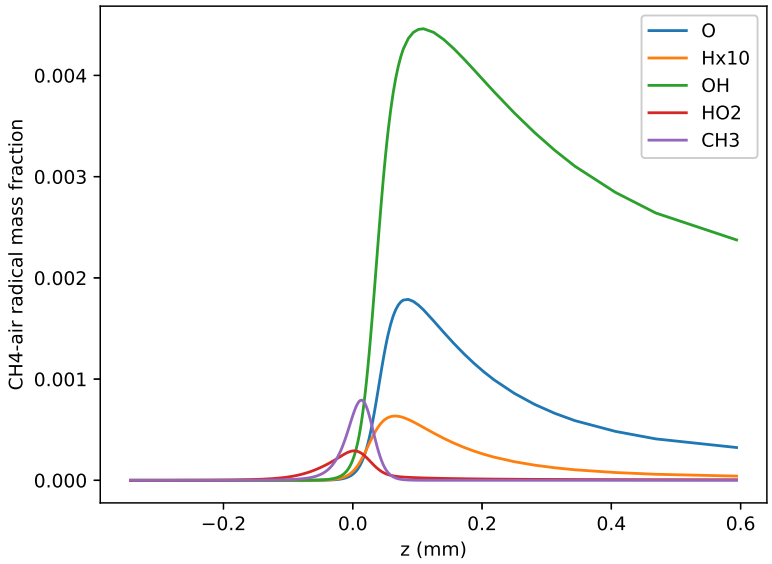

Figure 8: Reaction radicals for a methane-air laminar flame with T_0=800K, p=4 atm, ϕ=0.7.

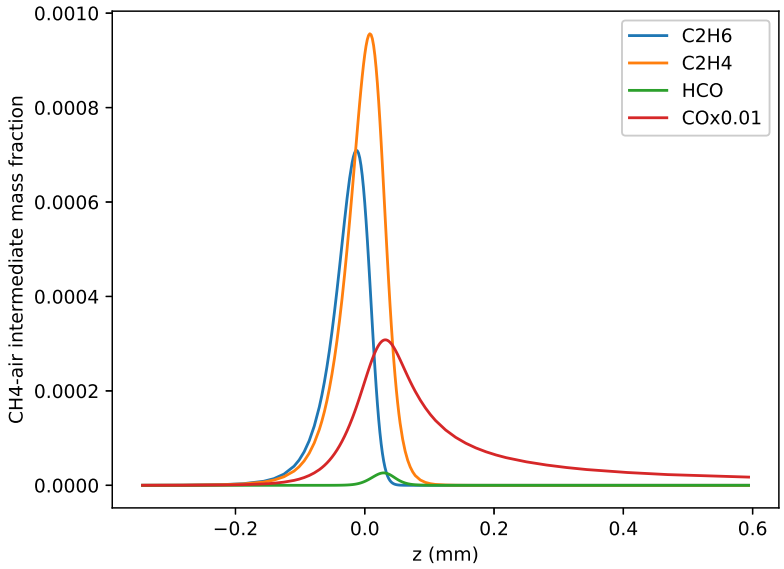

Figure 9: Reaction intermediates for a methane-air laminar flame with T_0=800K, p=4 atm, ϕ=0.7.

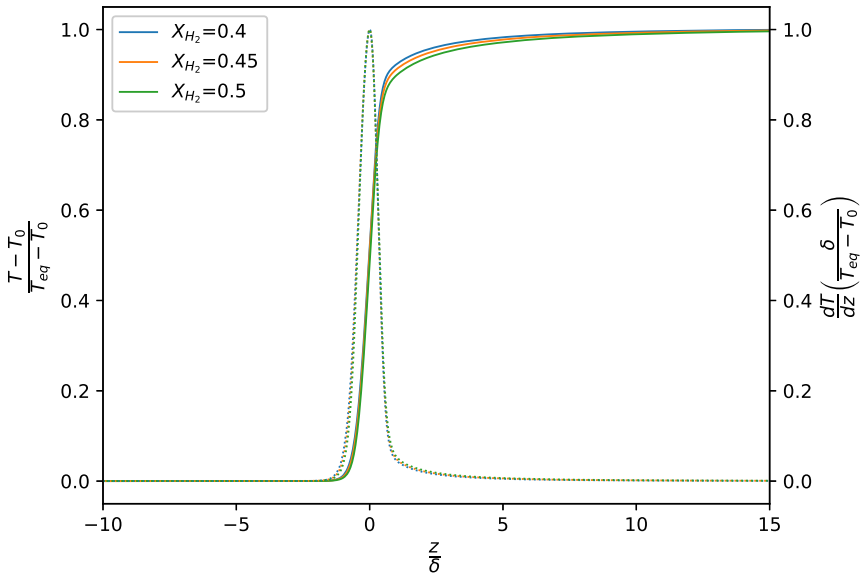

Figure 10: Temperature profile for a methane-air laminar flame with $T_0 = 800$ K and $p = 4$ atm at multiple equivalence ratios.

The flame temperature is normalized by

$$T_{norm} = \frac{T - T_0}{T_0 - T_{eq}}. \tag{17}$$

The grid coordinate, z, is nondimensionalized by the flame thickness

$$z_{norm} = \frac{z}{\delta}. \tag{18}$$

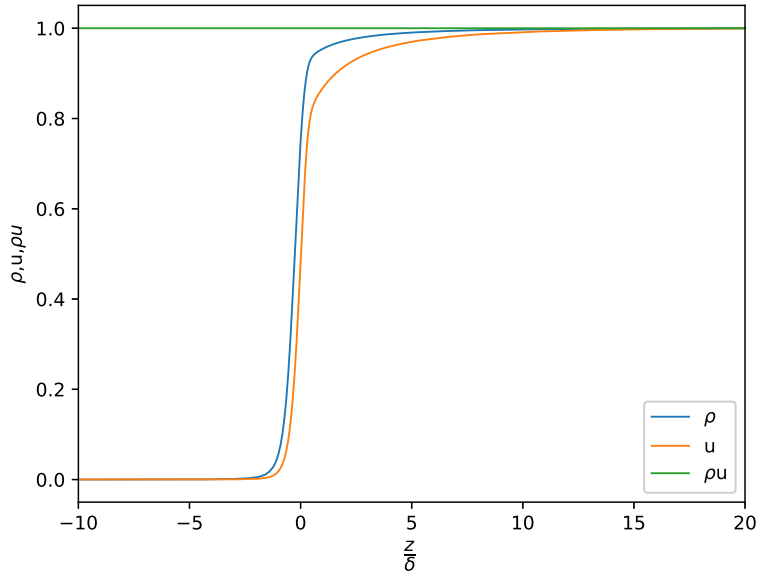

Figure 11: ρ, u, ρu for a methane-air laminar flame with T_0=800K, ϕ=1.0, and p=4 atm.

The gas density ρ is normalized by

$$\rho_{norm} = \frac{\rho - \rho_0}{\rho_0 - \rho_{eq}}, \tag{19}$$

where ρ_0 is the unburned gas density and ρ_{eq} is the flame density.

The laminar flame speed u is normalized by

$$u_{norm} = \frac{u - u_0}{u_0 - u_{eq}}, \tag{20}$$

where u_0 is the unburned velocity and u_{eq} is the laminar flame speed.
ρu, or $\dot{m}$, is the flow rate of reactants into the flame. The mass flow rate $\dot{m}$ is normalized by

$$\rho u_{norm} = \frac{\rho u}{\rho u}. \tag{21}$$

Figure 3 shows the specific enthalpy per unit mass of the flame. I edited the methods processFlame and writeFlame within the uberFlame.py class to calculate enthalpy.

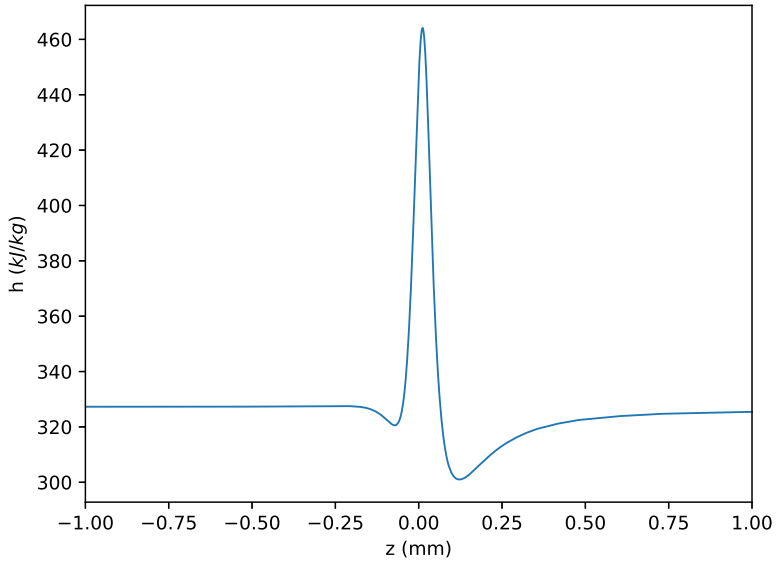

Figure 12: Specific enthalpy per unit mass for a methane-air laminar flame with T_0=800K, ϕ=1.0, and p=4 atm.

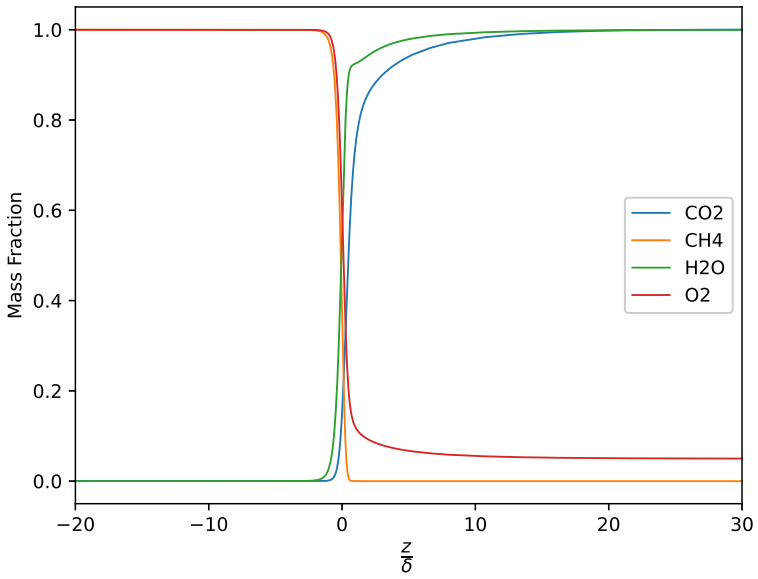

Figure 13: Reactants and products for a methane-air laminar flame with T_0=800K, ϕ=1.0, and p=4 atm.

Mass fractions for reactants are normalized by

$$Y_{react} = \frac{Y_{react}}{Y_i}, \tag{22}$$

where Y_i is the initial mass fraction of the reactant, while mass fractions for products are normalized by

$$Y_{prod} = \frac{Y_{prod}}{Y_{eq}}, \tag{23}$$

where Y_{eq} is the equilibrium mass fraction of the products.

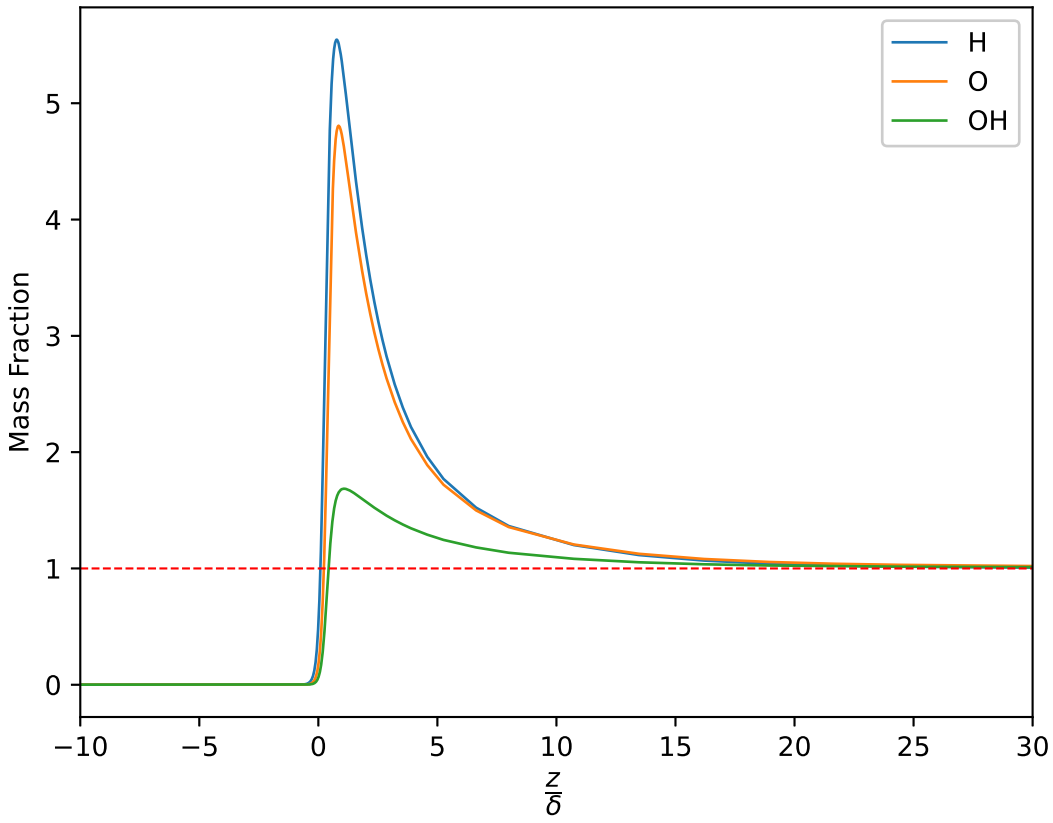

Figure 14: Combustion radicals for a methane-air laminar flame with T_0=800K, ϕ=1.0, and p=4 atm.

The mass fractions for the radicals are normalized by

$$Y_{rad} = \frac{Y_{rad}}{Y_{eq}}. \tag{24}$$

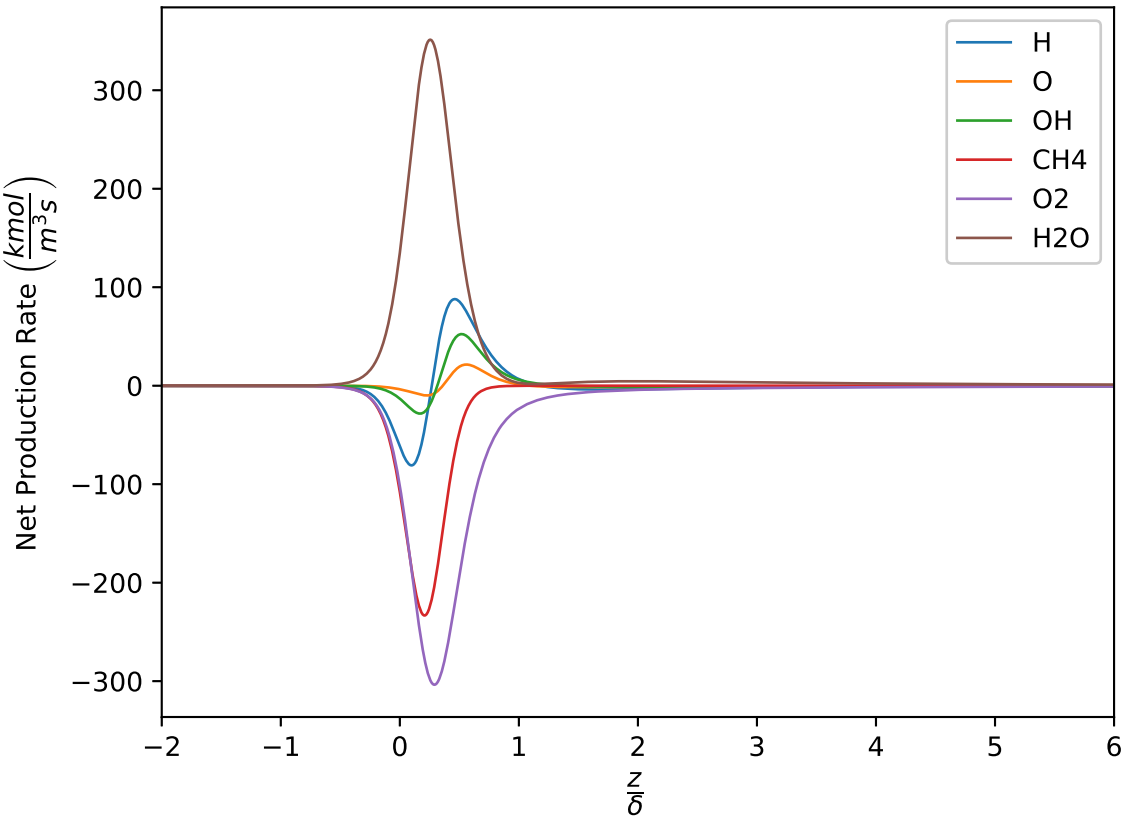

Figure 15: Net molar production rates for a methane-air laminar flame with T_0=800K, ϕ=1.0, and p=4 atm.

5 Spatial and Temporal Convergence

We find that x points in the thermal thickness are required to spatially resolve the grid. The mass flux of a flame vs a single spatial coordinate at an instantaneous point in time is calculated. In previous work, it was determined that this error resulted from using a coarse grid with 200 points across the spatial axis with 4.33 grid points in the thermal thickness.

This was enough to resolve the flame density, but not the velocity, resulting in an underestimation of the mass flux at the center of the flame, as seen in Figure 16. This week, the mesh is refined further, where h is defined as

$$h = \frac{\delta_t}{N}, \tag{25}$$

where δ_t is the flame thermal thickness and N is the number of grid points used in the computational domain.

The flame data from NGA and Cantera is shifted so that the corresponding flame datasets reach a common reference temperature T = 1000 K at x = 0.

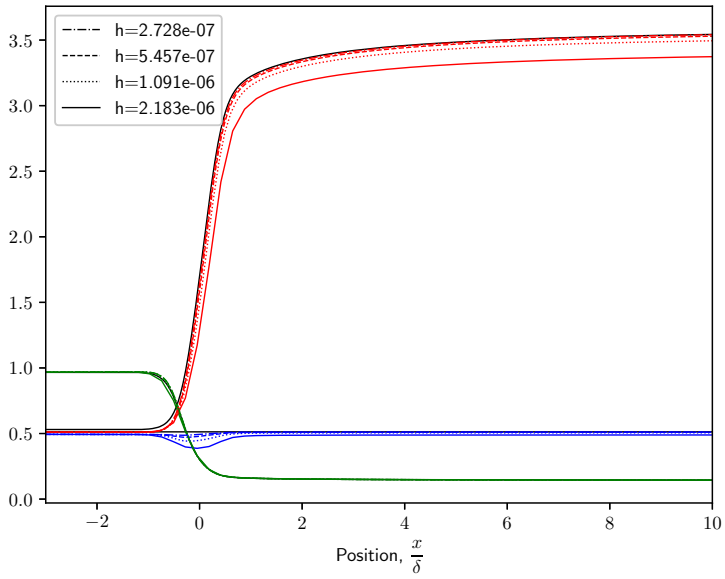

Figure 16: Velocity, mass flux, and density for a simulation of a NH_3/H_2 flame with $\phi = 1.0$, $\gamma = 0.5$, P = 1.0 atm, and T_0 =298.15 K. The solid black lines are from Cantera, while the red lines are from NGA simulated with increasingly finer meshes.

The heat release rate HRR_j ($\frac{J}{m^3 s}$) vs one spatial coordinate x_j is defined as

$$HRR_j = \Sigma_{i=0,j}^{N-1} K_{ij} h_{ij} \tag{26}$$

where N is the number of species, K_{ij} is the net production rate for each species (mol/m^3s) and h_{ij} is the specific enthalpy per unit mole for each species (J/mol).

The steady flame temperature over the domain at an instantaneous point in time is taken from NGA, along with a list of species mole fractions. Cantera is then used to compute the net production rates and specific enthalpies from the data.

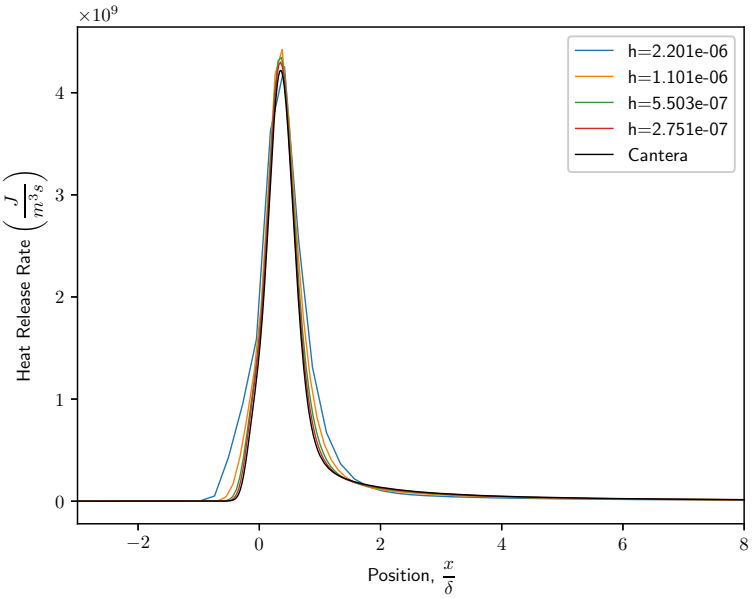

Figure 17: Heat release rate of a NH_3/H_2 flame with $\phi = 1.0$, $\gamma = 0.5$, P = 1.0 atm, and T_0 =298.15 K. Results from NGA postprocessed with Cantera at various values of h are compared against results from Cantera.

Figures 16 and 17 show that as the grid is refined, the discrepancy between the data from Cantera and from NGA decreases.

There appears to be diffusive error at the peak heat release rate and little to no dispersive error overall. Although it seems that reducing the grid spacing and the timestep increases the accuracy of the solution, this may not be the most efficient method.